Wireless energy transfer system for use in underground mining

Przemysław DEJA[1], Marcin SKÓRA[2]*, Krzysztof STANKIEWICZ[3], Jarosław TOKARCZYK[4], Marcin KASPRZAK[5], Zbigniew KACZMARCZYK[6] and Robert HILDEBRANDT[7]

Authors' affiliations and addresses:

[1] KOMAG Institute of Mining Technology, Pszczyńska 37, 44-101 Gliwice, Poland
e-mail: pdeja@komag.eu

[2] KOMAG Institute of Mining Technology, Pszczyńska 37, 44-101 Gliwice, Poland
e-mail: mskora@komag.eu

[3] KOMAG Institute of Mining Technology, Pszczyńska 37, 44-101 Gliwice, Poland
e-mail: kstankiewicz@komag.eu

[4] KOMAG Institute of Mining Technology, Pszczyńska 37, 44-101 Gliwice, Poland
e-mail: jtokarczyk@komag.eu

[5] Silesian University of Technology, Power Electronics Electrical Drives and Robotics Department (KENER), Krzywoustego Str. No.2, 44-100 Gliwice, Poland
e-mail: marcin.kasprzak@polsl.pl

[6] Silesian University of Technology, Power Electronics Electrical Drives and Robotics Department (KENER), Krzywoustego Str. No.2, 44-100 Gliwice, Poland
e-mail: zbigniew.kaczmarczyk@polsl.pl

[7] Central Mining Institute Experimental Mine "BARBARA", Underground Research and Surface Maintenance Dept., Podleska 72, 43-190 Mikołów, Poland
e-mail: rhildebrandt@gig.eu

*Correspondence:
Marcin Skóra, KOMAG Institute of Mining Technology, Pszczyńska 37, 44-101 Gliwice, Poland
tel.: +48 32 23 74 407
e-mail: mskora@komag.eu

Abstract

This paper presents the selected aspects of the research and development work carried out under the HEET II (High Efficiency Energy Transfer) project, supported by the Research Fund for Coal and Steel (RFCS). First, the concept of a system for wireless energy transfer using capacitive coupling is presented. Technically similar solutions, assumptions, selected results of model tests and main components of the system are presented, also connections to cooperating systems are described. An example of a machine adapted to receive energy from the discussed system has been shown. Moreover, the selected research aspects, which require special attention during testing the prototype, regarding the planned implementation, are detailed. The authors focused on the experimental determination of capacitive coupling parameters - the results indicate that it will be possible to meet the requirements of the power transfer in the planned prototype system.

Keywords

rail transport, battery-powered drivetrain, capacitive coupling, electric power supply, wireless power supply

Introduction

Transport processes are one of the basic processes in mines. A distinction is made between vertical and horizontal transport. By their means not only employees, but also the excavated material and equipment are transported. Due to the wide variety of transported materials, technical conditions and length of the routes, suitable means of transport are used. Suspended drivetrains moving along a route built of steel profiles are one of these means, selected for testing within the HEET II project. These drivetrains use different types of following propulsion systems: pneumatic, hydraulic, electric, diesel or hybrid. The first three of these can be zero-emission drives whose operating time, range and power are limited by the parameters of the energy accumulator used or the length of the supplying cable (Konsek, Kaczmarczyk, Budzyński, & Polnik, 2013; Stankiewicz 2020). Increasing the capacity of energy accumulators is not always possible due to their weight and cost. Therefore, it would be advantageous to provide the possibility of replenishing the energy in the battery while the drivetrain is in operation. As the machine runs in methane and/or coal dust explosive atmospheres, the energy transfer should be wireless. Basic types of wireless energy transfer solutions are known - with inductive and capacitive coupling. The first one uses magnetically coupled coils. Such systems are well known and applied for charging batteries in consumer electronics (e.g. mobile phones), biomedical implants or electric vehicles (Jeong, Park, Hong, & Rim, 2019; Zhang, Pang, Georgiadis, & Cecati, 2019). Some systems of this type are envisaged to work with vehicles while they are in motion (Mi, Buja, Choi, & Rim, 2016; Mohammed & Jung, 2021; Zhang, Lu, & Mi, 2020). The paper (Zhang, Lu, & Mi, 2020) provides a comprehensive overview of different vehicle charging methods. The solution with inductive energy transfer cannot be used in mining conditions, due to the possibility of heating up of metal objects that would be located near the cooperating coils and thus creating an explosion hazard. Hence, attention has turned to the systems with capacitive coupling, which in recent years have become the object of increasing testing and implementation (Kracek & Svanda, 2019; Regensburger et al., 2018; Sinha, Kumar, & Afridi, 2018; Zhang, Zhu, & Lu, 2019). Some of these solutions involve the use of capacitive coupling for charging vehicles in motion (Mohammed & Jung, 2021; Zhang, Lu, & Mi, 2020; Maji, Sinha, & Afridi, 2021; Vu, Dahidah, Pickert, & Phan, 2020 Hanazawa, Sakai, & Ohira, 2012). These papers focus on issues relating to the shape of the transmitter and receiver, or the choice of operating frequency. In (Vu, Dahidah, Pickert, & Phan, 2020; Zhang, Lu, & Mi, 2020), solutions, where the transmitter and receiver electrodes are in plate form, where the transmitter plate can be placed along the road. are described. The basic solution involves the use of two capacitively coupled plates (transmitting and receiving), while the systems with four or six plates are also possible, with additional plates acting as screens (Zhang, Lu, & Mi, 2020). In (Maji, Sinha, & Afridi, 2021) it was proposed that the transmitting electrodes should be placed along the road, as discrete devices, at short distances from each other. On the other hand, in (Hanazawa, Sakai, & Ohira, 2012), it was proposed that a transmitting electrode in the form of a plate placed in the roadway works together with a receiving electrode placed in a car tyre. The work cited focuses on the systems operating at several megahertz and 13.56 MHz.

The proposed concept of Capacitive Wireless Energy Transfer (Capacitive WET) is shown in Fig. 1. The system consists of:

- an energy transmitter comprising a converter with a high frequency output voltage, with a step-up transformer,
- two capacitors, responsible for capacitive coupling (C1, C2),
- an energy receiver, with a step-down transformer and a rectifier, to supply the battery charger (battery charging).

Each of the capacitors referred to above consists of two plates. One of these plates, the shorter one (receiving), moves together with the machine (the suspended drivetrain). The other (transmitting) is longer and is installed into the suspended rail. In order to make this possible, the rail of the route has to be developed in a special way. Instead of metal rails, composite rails were proposed, with a suitable dielectric layer at the point forming a capacitor.
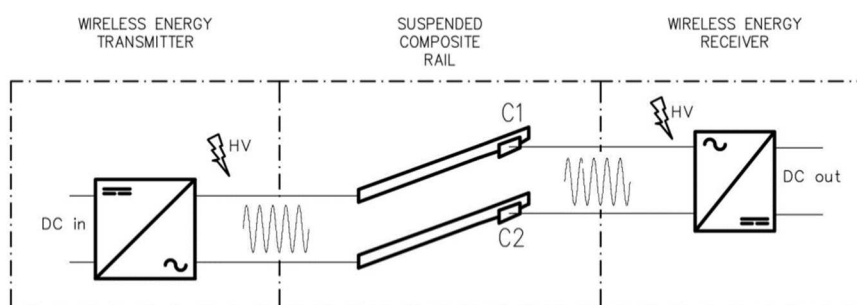

Fig. 1. Concept of energy transfer in a WET system with capacitive coupling

The solution described in the paper is an attempt to develop an innovative method for supplying power to electrical machines and equipment operating in underground mine workings, including those with methane and/or coal dust explosion hazards. Despite a number of potential advantages, such as high efficiency, safety of use, wireless transfer of energy to moving receivers, the authors have not found similar devices in the underground mining industry, which may be due to the potentially high costs of development and approval when it comes to this solution. The suggested system is under development and its testing is as part of the research project *Innovative high efficiency power system for machines and devices increasing the level of work safety in underground mining excavations*, financed by the Research Fund for Coal and Steel (RFCS). The acronym of the project is HEET II: High Efficiency Energy Transfer. The new innovative power supply system will consist of the following several cooperating components:

- the Wireless Energy Transfer (WET) system, as conceptualized in Fig. 1,
- composite rails, including capacitor plates, used in the WET system,
- the SWET (Single Wire Energy Transfer) system (Zygmanowski et al., 2021), which is the power source for the WET system,
- a wire and wireless communication system, together with appropriate sensors for monitoring environmental parameters (Kianfar et al., 2022) and a low-power wireless power supply,
- a sample machine - in the form of a suspended drivetrain, powered by the WET system (Konsek, 2012; Konsek, Kaczmarczyk, Budzyński, & Polnik, 2013),
- a database storing information enabling the analyses of operation of the entire system.

The overall conceptual block diagram of the HEET II power system is shown in Fig. 2 below. In this diagram, the described WET system is marked.
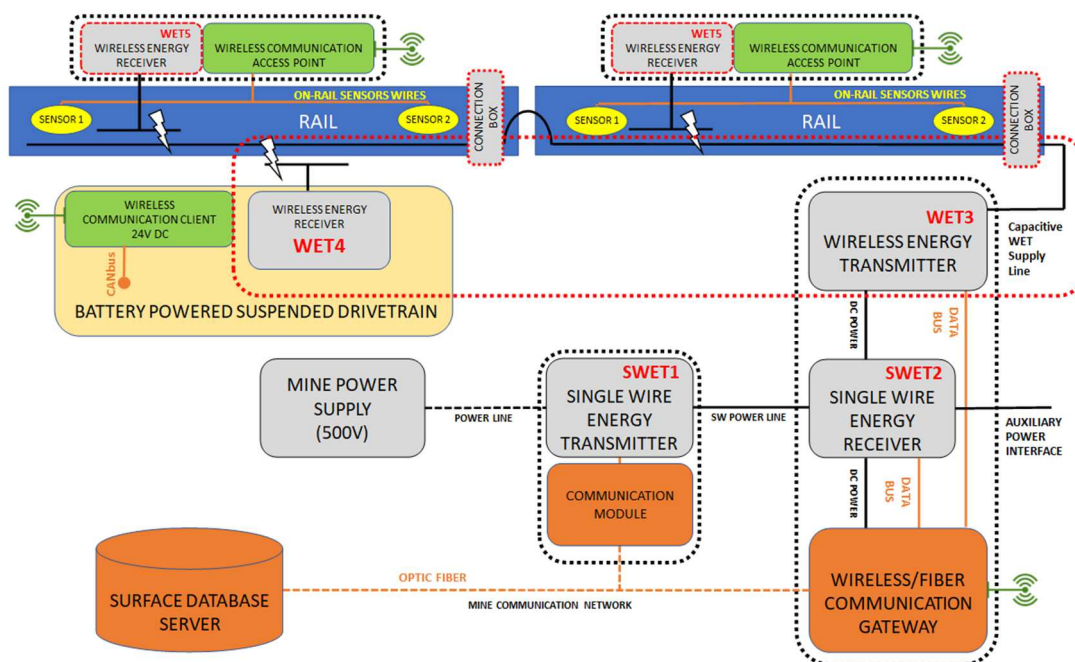

Fig. 2. Concept for an innovative power supply system being developed within the HEET II project

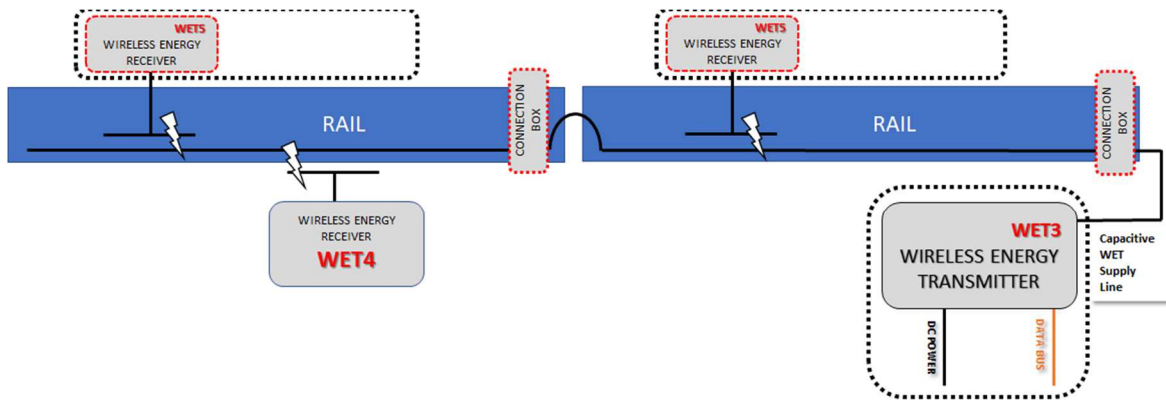The components of this system are given in Fig. 3.

Fig. 3. Concept of the WET system

A suspended PCA-1 battery drivetrain (Konsek, 2012; Konsek, Kaczmarczyk, Budzyński, & Polnik, 2013) was selected for testing the WET system as the energy-consuming machine. This drivetrain (shown in Fig. 4) is designed for manoeuvring work related to the movement of transport sets on a suspended rail in a roadway. It can be used in areas threatened by methane and/or coal dust explosion, including underground mines of coal, ore, salt and other useful minerals, in the areas with methane explosion hazard and coal dust explosion hazard. This drivetrain was selected as a technology demonstrator within the HEET II project, while ultimately the WET system's receiving module will be tailored to the specific working machine.

Fig. 4. Suspended battery drivetrain to be used as an example of a machine powered by wireless energy transfer

Power of each of two electric motors used to power the drivetrain, as well as each of two hoist motors, was 1.1 kW. Taking into account the power consumed by the control and auxiliary equipment, the nominal power of the suspended drivetrain can be estimated as P_{tN}=2.5 kW. On this basis, the minimum nominal power transmitted wirelessly to the drivetrain (including the charging battery) equal to $P_{WET,N}$=2 kW was assumed. An additional argument for this design assumption is the fact that systems with capacitive coupling are generally suggested for low power systems, up to 2 kW (Regensburger et al., 2018). Ultimately, the WET system will allow scaling of the transmitted power depending on the application.

In order to meet the assumptions made above for the power of WET system, appropriate calculations were made to estimate the key system parameters. In general, for voltage-fed systems with low capacitive couplings, the maximum power available during energy transfer is proportional to the coupling capacitances (lower coupling reactances and higher currents), the switching frequency (lower coupling reactances and higher currents), and the square of the supply voltage (voltages and currents of the system proportional to this voltage) (Zhang, Lu, & Mi, 2020). Due to the small coupling capacitances in the design of the component devices, the presence of voltage step-up and step-down transformers. was taken into account in the design of the component devices. The selected results of calculations are given in Tab. 1.

As shown in Tab. 1, high voltage U_{HV3} is one of the quantities that characterises the operation of a WET system. This voltage supplies the plates, which form the capacitors in the composite rails. This voltage will have a great impact on the materials and insulation distances used. Increasing the voltage on a high-frequency line reduces the transmitted current, which translates into an increase in load resistance, important from the point of view of the efficiency of energy transfer. Relevant comments will be given in Section 4.1.

Tab. 1. Assumed parameters of the WET system

No	Parameter	Value	Description
1	U_{DC23}	(750- 870) V DC	WET3 – supply voltage form SWET2
2	f_3	50 kHz min	WET3 switching frequency
3	U_{HV3}	up to 10 kV AC	HVHF line RMS voltage
4	$I_{HV3} \approx I_{HV4}$	(0.3-0.5) A AC	HVHF line RMS current (2.3 kW load)
5	C_1, C_2	≈300 pF	C_1 and C_2 capacitances, approximate values
6	P_{BAT}	up to 2 kW	Battery charging power

HVHF – High Voltage High Frequency

One of the reasons for undertaking the task of developing the WET system is the limited runtime of the drivetrain battery due to the limited capacity of the batteries used in them. In the case of the drivetrain selected as a prototype, the built-in lithium-iron-phosphate batteries have a capacity of 5.76 kWh. This allows, theoretically, for about 2.25 hours of drivetrain operation at full load P_{tN}=2.5 kW, taking into account the power of the drive motors and the operation of auxiliary equipment. Equipping a suspended drivetrain with an additional receiving module, allowing the drivetrain to be powered and its batteries to be recharged anywhere along the suspended rails, will allow the working time to be extended. It is important that this time can exceed the length of the work shift. In cases, where the averaged power consumed by the drivetrain P_t is less than the power P_{WET} supplied by the wireless energy transfer system, even breaks for charging the drivetrain's battery can be eliminated (e.g. for cases, where P_t=0.75 P_{tN} & P_{WET}=$P_{WET,N}$ and P_t=0.75 P_{tN} & P_{WET}=$P_{WET,N}$). Fig. 5a shows the results of a simplified simulation, showing the amount of energy stored in the battery, depending on the power consumed by the drivetrain and the power supplied by the WET system. On this basis, Fig. 5b presents how much the battery operating time (t) of this drivetrain will theoretically increase. This shows that increase in operating time can be significant, in some cases allowing uninterrupted operation during the entire working shift (an increase of several hours). During the operation of the battery drive, supervision of the battery should be ensured through the use of a BMS with a proper method of balancing the voltages on individual cells (Kurpiel, 2020), so that the theoretical extension of operating time through the use of WET subsystem is also realizable in practice.
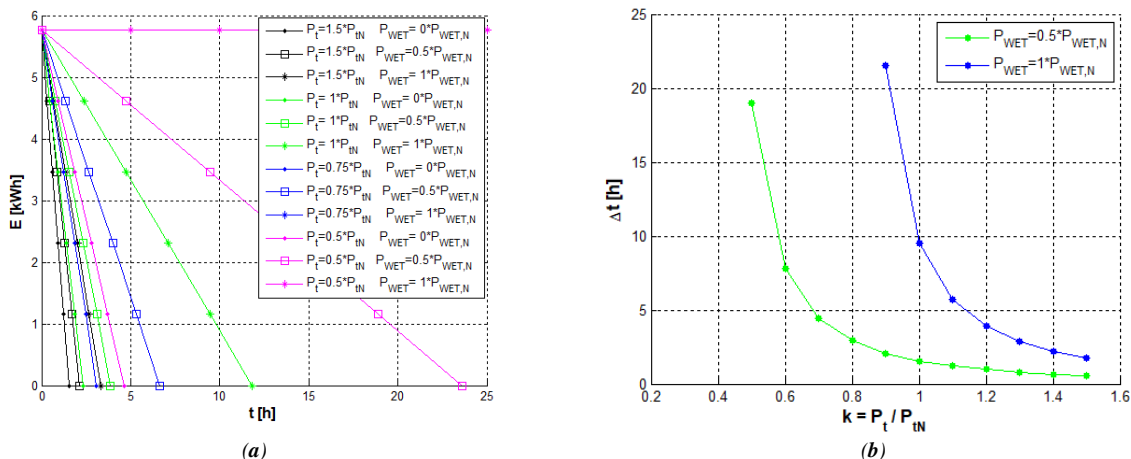

(a)   *(b)*

Fig. 5. Results of a simplified simulation: (a) change in remaining energy in the battery during operation, depending on the drivetrain load and the extracted power from the WET system ($P_{WET,N}$=2 kW, P_{tN} = 2.5 kW), (b) extension of the battery operating time, depending on the drivetrain load, for different levels of power from the WET system ($P_{WET,N}$=2 kW, P_{tN} = 2.5 kW)

Development of capacitive coupling is one of key elements that is required to develop a WET system to operate at its intended power is. Hence, it is crucial to know the parameters of capacitors formed by copper plates placed in a composite dielectric. This paper presents the results of preliminary tests to determine the properties of the capacitive coupling and to verify the assumption for the predicted power flow in a WET system.

Materials and Methods

A simplified capacitive WET system is presented in Fig. 6. The system consists of a supply source (a resonant inverter), two capacitors (formed by supply electrodes, dielectrics, and load electrodes), and a load (a rectifier with a load). The capacitors, independently of each other, form basic capacitors. In turn, both these capacitors, placed next to each other, create capacitive couplings and are the important part of the capacitive WET system.

First, initial experimental tests of the capacitive WET system consider a representative basic capacitor and then an entire configuration of the capacitors with their couplings.
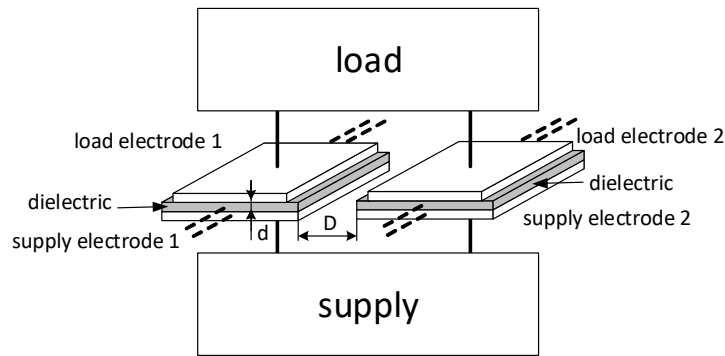
Fig. 6. General view of a capacitive WET system

Initial experimental identification of capacitive WET system parameters

Photos of the tested base capacitor are included in Fig. 7. The capacitor is made of copper plates (each 10 cm x 100 cm and a thickness of 0.1 mm) and a composite dielectric layer (glass mat with epoxy resin) with or without an additional air gap – for this test, one of the capacitors shown in Fig. 6a was used.
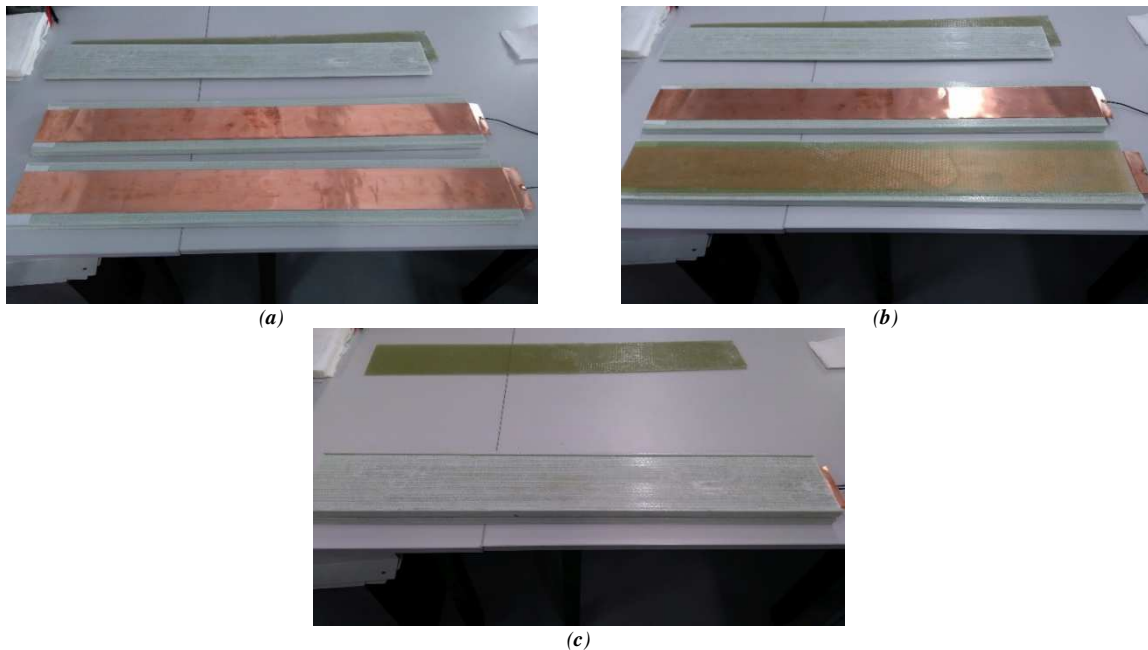

(a)

(b)

(c)

*Fig. 7. Basic capacitor: (a) disassembled, (**b**) with a composite dielectric,(**c**) assembled – ready for measurements*

For the measurements a precise Agilent 4294A impedance analyser was used in various configurations of the dielectric layer and / or air gap, several distances between the copper plates (*d, d_0, d_d* in Fig. 8) and frequencies.
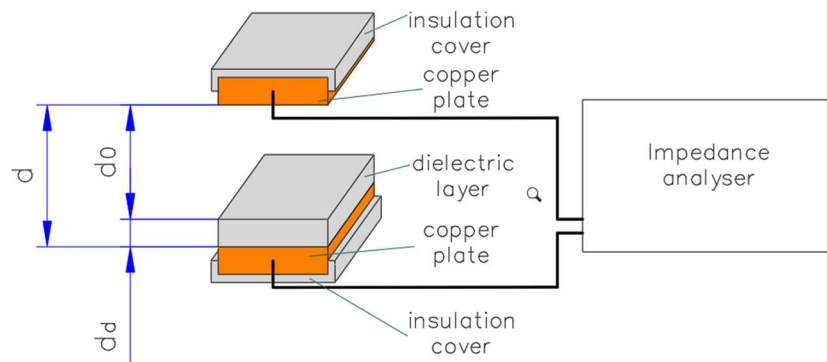

Fig. 8. Measuring scheme

Capacitive couplings

Main capacitors formed by the supply electrodes, dielectrics, and load electrodes are very important components of capacitive WET systems. In the considered case, the supply electrodes are relatively long, many times longer than the receiving electrodes (Fig. 1, Fig. 6). The two receiving electrodes slide along the supply electrodes to ensure wireless energy transfer. The corresponding electrodes have an analogous design. Unfortunately, such a solution creates additional parasitic capacitances having some negative impact on the properties and parameters of the WET system. In simplified form, the main and parasitic capacitances are depicted in Fig. 9. Determining these parameters is essential for the designing process.
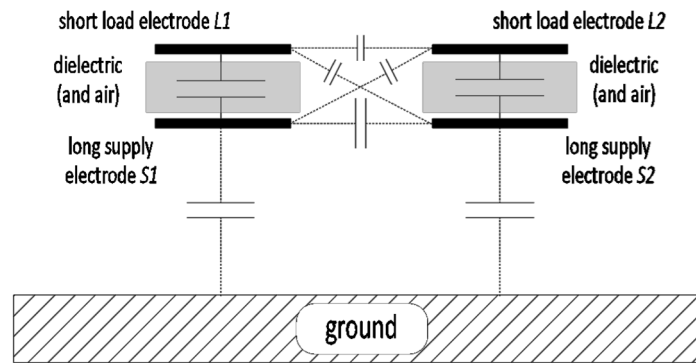

Fig. 9. Main capacitors and parasitic capacitances of capacitive WET system

The capacitive couplings from Fig. 9 can be represented by a four-terminal network (Fig. 10), which at this stage is sufficient to determine representative properties of the WET system. The network is assumed to include two main identical series of capacitors C_S (each corresponding to the base capacitor) and one parallel capacitance C_P (containing all parasitic capacitances). Initially, due to the low measurement accuracy of equivalent series resistances (dominant capacitive nature), they are omitted. Taking these resistances into account will be necessary in the next step to determine power losses of the WET system. The final simplified schematic diagram is depicted in Fig. 11.
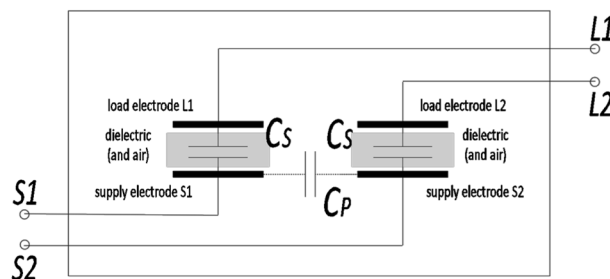

Fig. 10. Simplified representation with two main capacitances and one parasitic capacitance as four-terminal network
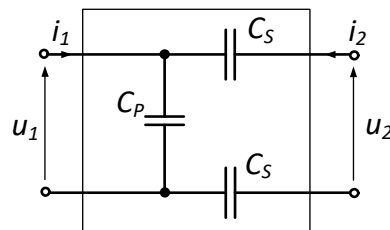

Fig. 11. Simplified scheme with essential components

The laboratory setup to establish the four-terminal network parameters from Fig. 11 is illustrated in Fig. 12. The short receiving electrodes are made of copper plates (10 cm x 100 cm and a thickness of 0.1 mm). In the experimental validation, the composite dielectric layers forming 7 mm distance between the electrodes were used. The supply electrodes are 10 m long. Since only two parameters (capacitances) are unknown, two measurements are sufficient. More measurements were made to verify the presented concept in more detail. The measurement frequency is set to 50 kHz.
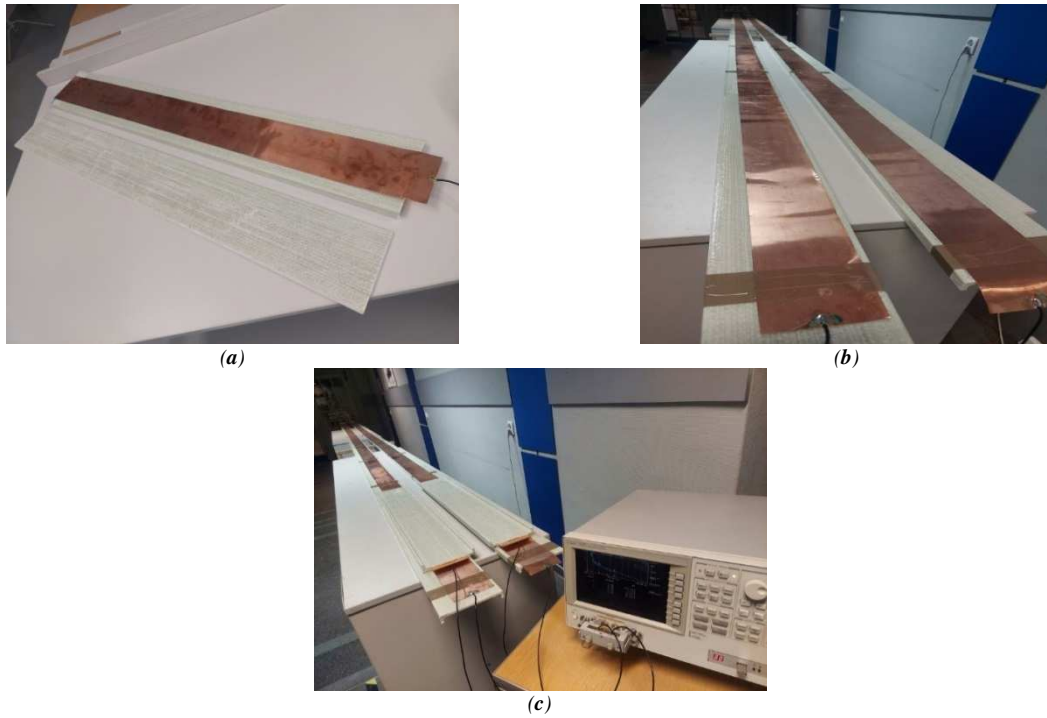
(a)

(b)

(c)

*Fig. 12. View of: (**a**) short load electrode and dielectric layer, (**b**) long supply electrodes,*
*(**c**) laboratory setup ready for measurements*

Results

Initial experimental identification of capacitive WET system parameters

The results of measurements for various configurations of the dielectric layer and/or air gap, several distances between the copper plates and frequencies are presented in the form of example characteristics (Fig. 13-Fig. 15) and a quantification in Tab. 2. Equivalent electrical parameters C_S-R_S are determined corresponding to a series connection of capacitor and resistor.
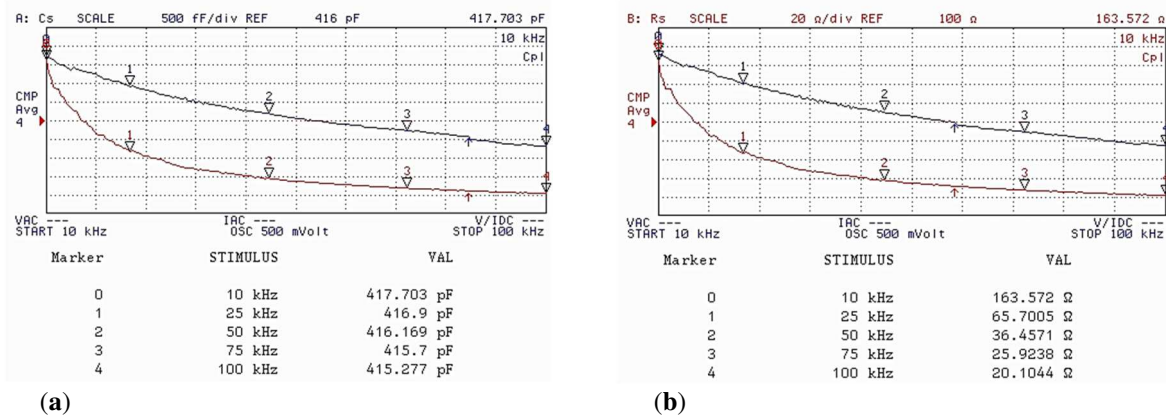

(a)

(b)

*Fig. 13. Equivalent capacitance C_S (**a**) and resistance R_S (**b**) for the distance of*
7 mm (only dielectric layer) as a function of the frequency

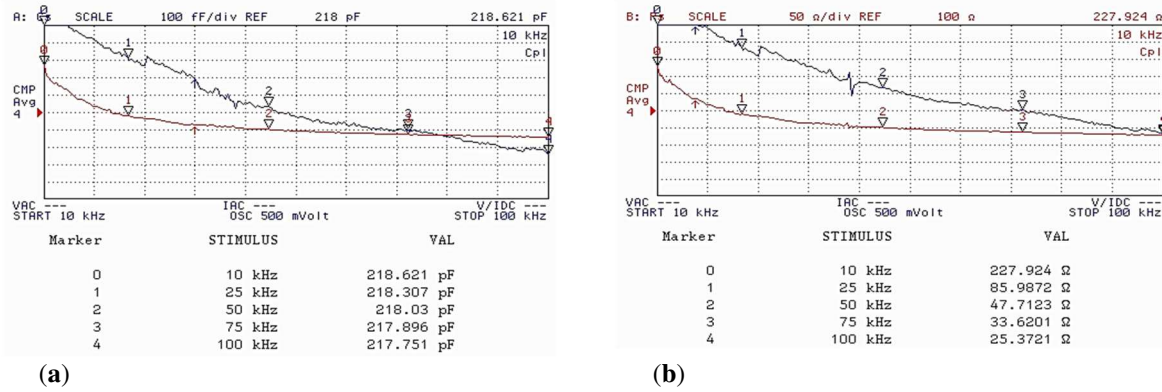(**a**)   (**b**)

*Fig. 14. Equivalent capacitance C_S (**a**) and resistance R_S (**b**) for the distance of*
7 mm (dielectric layer) and 3 mm (air gap) as a function of the frequency

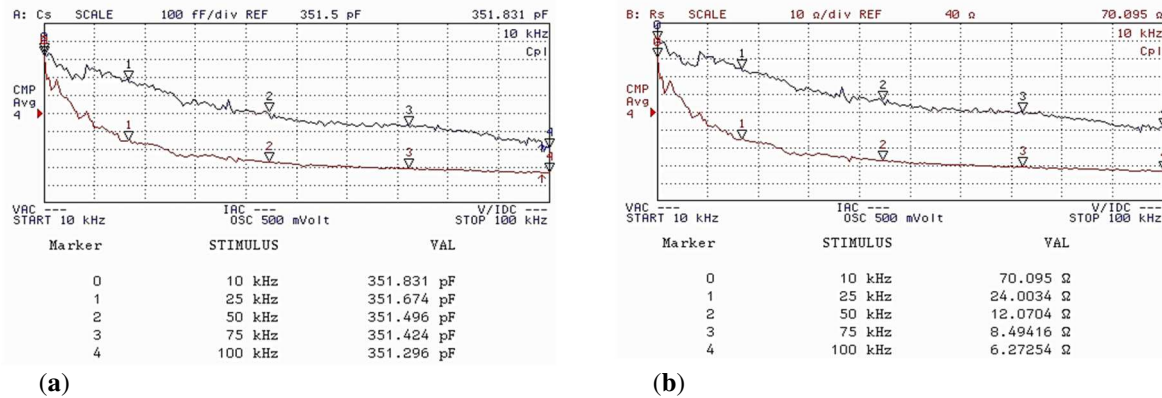(**a**)   (**b**)

*Fig. 15. Equivalent capacitance C_S (**a**) and resistance R_S (**b**) for the distance of 3 mm (only air gap) as a function of the frequency*

The representative measurements for the frequency of 50 kHz are listed in Tab. 2. It should be explained that the capacitive reactance component is dominant. For example, for the frequency of 50 kHz and the capacitance of 416 pF, the capacitive reactance is 7.7 kΩ and is much higher than the series resistance of 36 Ω. As a result, in all cases, the series capacitances are measured more accurately, and the measurements of the series resistances are highly uncertain.

Tab. 2. Equivalent series parameters of the base capacitor for 50 kHz

No.	Dielectric layer (mm)	Air gap (mm)	Capacitance (pF)	Resistance (Ω)
1	4	–	588	26
2	7	–	416	36
3	11	–	276	59
4	18	–	185	90
5	7	3	218	48
6	7	6	141	52
7	7	12	90	76
8	–	3	351	12
9	–	6	185	17
10	–	12	101	51

Tab. 3 summarizes the base capacitor parameters, allowing for some generalizations. Using the following relationship for the capacitance of a flat capacitor:

$$C_S = \frac{\varepsilon_0 \varepsilon_r S}{d}, \quad C_{cal} = \frac{\varepsilon_0 S}{d},$$ (1)

where:
$\varepsilon_0 = 8.854 \cdot 10\text{-}12$ F/m – permittivity of vacuum,
ε_r – relative permittivity,
S – area of capacitor copper plates ($S = 1$ m $\cdot$ 0.1 m = 0.1 m^2),
d – distance between the plates containing the dielectric layer d_d and the air gap d_0
($d = d_d + d_0$, (m)),

the capacitances of the corresponding air capacitor C_{cal} (no. 1-4) and (no. 8-10) are calculated. Then, based on:

$$\varepsilon_r = \frac{C_S(d)}{C_{cal}(d)}, \tag{2}$$

the relative permittivity ε_r (no. 1-4 in Tab. 3, for a given dielectric layer and no. 8-10 in Tab. 3 for a given air gap) was found. Finally, the equivalent capacitances C_{S_cal} and resistances R_{S_cal} (capacitors no. 5-7) are calculated, resulting directly from a series connection of the measured capacitances C_S and resistance R_S, according to (no. 2) and (no. 8-10):

$$C_{S\_cal} = \frac{C_S(d_d=7mm)\cdot C_S(d_0)}{C_S(d_d=7mm)+C_S(d_0)}, \quad R_{S\_cal} = R_S(d_d = 7mm) + R_S(d_0), \tag{3}$$

These results make it possible to compare the obtained parameters C_{S_cal} and R_{S_cal} (no. 5-7) with the measured ones C_S and R_S (no. 5-7) for the simultaneous application of the dielectric layer and air gap. The results are consistent enough.

Tab. 3. Calculated parameters of the base capacitor for the frequency of 50 kHz
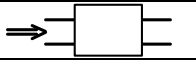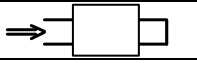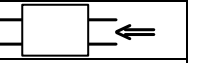
No.	d_d (mm)	d_0 (mm)	C_S / R_S (pF / Ω)	C_{cal} / ε_r (pF / –)	C_{S_cal} / R_{S_cal} (pF / Ω)
1	4	–	588 / 26	221 / 2.7	
2	7	–	416 / 36	126 / 3.3	
3	11	–	276 / 59	80 / 3.5	
4	18	–	185 / 90	49 / 3.8	
5	7	3	218 / 48	–	190 / 48
6	7	6	141 / 52	–	128 / 53
7	7	12	90 / 76	–	81 / 87
8	–	3	351 / 12	295 / 1.2	
9	–	6	185 / 17	148 / 1.3	
10	–	12	101 / 51	74 / 1.4	

Capacitive couplings

First, the capacitance of the base capacitor made of two short electrodes and 7 mm dielectric layer was measured (Fig. 12a). Next, the capacitance between the long electrodes without the short electrodes was measured (Fig. 12b). The following parameters were measured: C_S = 418 pF, C_P = 183 pF. Finally measurements of the input and output capacitances of the four-terminal network were taken (Fig. 12c). These results are given in Tab. 4. The arrow indicates the pair of electrodes connected to the Agilent 4294A impedance analyser. Letter "o" in the subscript indicates that the second pair of electrodes is not connected together (open circuit), while the subscript "s" indicates that the second pair of electrodes is shorted together (short circuit). The dominant capacitive reactance component of the measured impedance was confirmed each time – the impedance representation by serial or parallel equivalent circuits gave the same capacitance.

Based on the individually measured series (C_S) and parallel (C_P) capacitances, the appropriate input and output capacitances of the four-terminal network were calculated (Tab. 4).

Tab. 4. Capacitance measurements of the four-terminal network

Measurements	C_{S1S2-o} = 188 pF	C_{S1S2-s} = 371 pF	C_{L1L2-o} = 106 pF	C_{L1L2-s} = 209 pF
Calculations based on C_S and C_P	C_P = 183 pF	$C_P + \frac{C_S}{2}$ = 392 pF	$\frac{\frac{C_S}{2}\cdot C_P}{\frac{C_S}{2}+C_P}$ = 98 pF	$\frac{C_S}{2}$ = 209 pF

The direct measurements and calculations confirm the correctness of the assumptions – some cross-coupling parasitic capacitances can be omitted. The four-terminal network capacitances can be determined by measuring the entire circuit or applying the individual capacitance measurements of the base capacitor and long supply electrodes. During the measurements in the frequency range from 10 to 200 kHz, no significant frequency effect is observed.

The final scheme of the capacitive path of the WET system is shown in Fig. 16. It includes the series resistances related to main power losses and an equivalent load resistor. The resistances were measured in the base capacitor – for this case R_S = 36 Ω (Fig. 13). For sinusoidal voltage/current waveforms, in the symbolic domain, the input impedance is given as:

$$\underline{Z_I} = \frac{RX_P^2 - jX_P[R^2+X_S(X_P+2X_S)]}{R^2+(X_P+2X_S)^2}, \tag{4}$$

$$X_P = \frac{1}{\omega C_P}, \quad X_S = \frac{1}{\omega C_S}, \quad R = R_O + 2R_S, \tag{5}$$

The efficiency is expressed simply as:

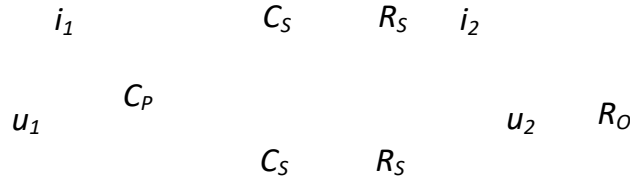$$\eta = \frac{1}{1 + 2\frac{R_S}{R_O}}.$$

(6)

Fig. 16. Simplified scheme with essential capacitances and additional series resistances and equivalent load resistor R_o

Equation (6) was visualised for different load resistance. The determined value of $R_S = 36\ \Omega$ and its multiples were assumed. It can be seen from Fig. 17 that the series resistance should be lowered and the load resistance should be increased to increase the efficiency of power transfer through the capacitive path of the WET system.
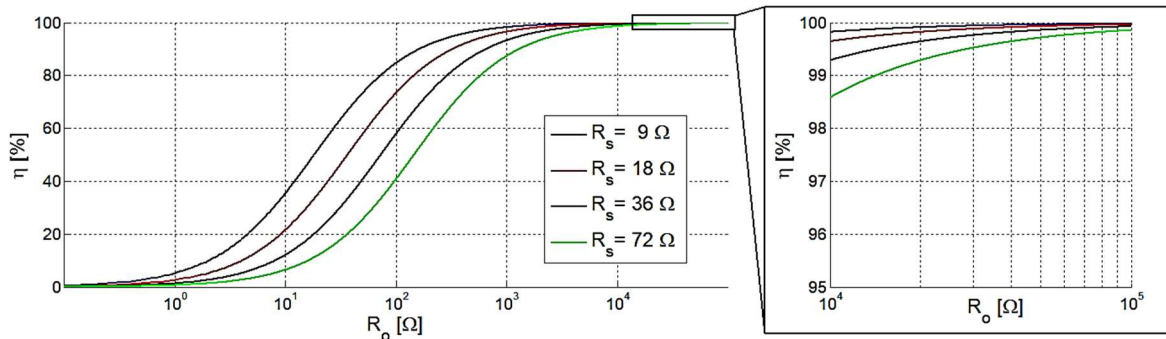

Fig. 17. Efficiency versus load resistance - visualisation of the relationship (6)

Discussion

Initial experimental identification of capacitive WET system parameters

The relative permeability of the composite dielectric is about 3. Some observed discrepancies are related to the measurement inaccuracy and the irregular shape of the base capacitor dielectric layer.

It was confirmed that the base capacitor of the capacitive WET system, containing a dielectric layer and air gap between the electrodes, can be treated as a series connection of two respective capacitors.

Air gaps determine the total capacitance of the base capacitor. The obtained capacitances are relatively small, which will make the wireless energy transfer difficult. It is necessary to determine the minimum possible distance between the electrodes of the base capacitor.

Considerations of capacitive couplings

It should be emphasized that the parallel capacitance C_P is proportional to the length of the supply electrodes. In turn, the series capacitance C_S is mainly the result of the geometry and electrical parameters of the base capacitor. For effective energy transfer, it is important to minimize the parallel capacitance C_P and the series resistance R_s, while maximizing the series capacitance C_S.

The relatively large parallel capacitance (close to the series capacitance) is a serious problem. Some improvement can be made by using parallel (parallel connection of a coil to the input) and/or series (serial connection of a coil to the output) compensation. The series resistance will decrease when a thicker copper sheet is used as the capacitor plates.

The efficiency of the overall energy transfer system developed in the HEET II project does not only depend on the efficiency of the energy transfer via the capacitor (Fig. 17), but also on the efficiency of the transformers and converters. The analyses carried out so far allowed to estimate the power losses related to the converters (Zygmanowski et al., 2021).

Conclusions

The results of preliminary tests related to the construction of a wireless energy transfer system, which is intended to power equipment in underground mine roadways were presented. The tests concerned one of the key components of WET, i.e. capacitors responsible for capacitive coupling between the energy transmitter and receiver.

The results presented above indicate that with careful selection of the composite material and maintaining a minimum air gap, it will be possible to achieve the required coupling capacitances and transmit the assumed 2 kW power wirelessly. Matching the resistance of the load (WET4 receiver) will in turn make it possible to achieve high system efficiency (see Fig. 17 for details). In this way, the requirements set for the WET system will be met.

The next stage will be to make comparative tests of the capacitive WET system supplied by a resonant inverter (with transformers and high voltage supply). They will enable more advanced verification of the presented concept, by including voltage/current waveform distortions as well as enable identification of actual sources of power loss of the WET system.

At the same time, a preparation of prototypes of the devices comprising the innovative power supply system is underway. Electrical schematics and 3D models of each component were developed (some of them are shown in Fig. 18). On this basis, a preliminary visualisation of the whole system developed within the HEET II project was prepared (Fig. 19).
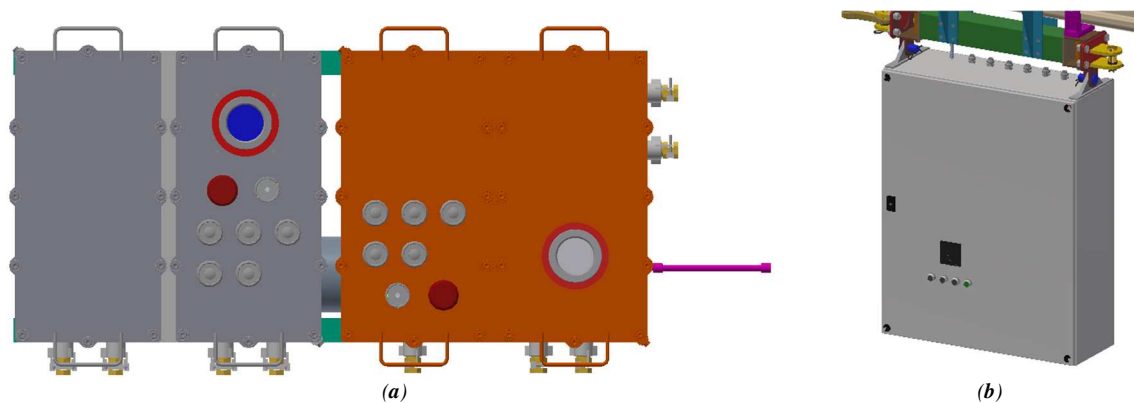

(a)   *(b)*

*Fig. 18. Visualisation of the enclosures: (**a**) for SWET2 (grey)/WET3 and communication (orange) systems, (**b**) for WET4 systems*
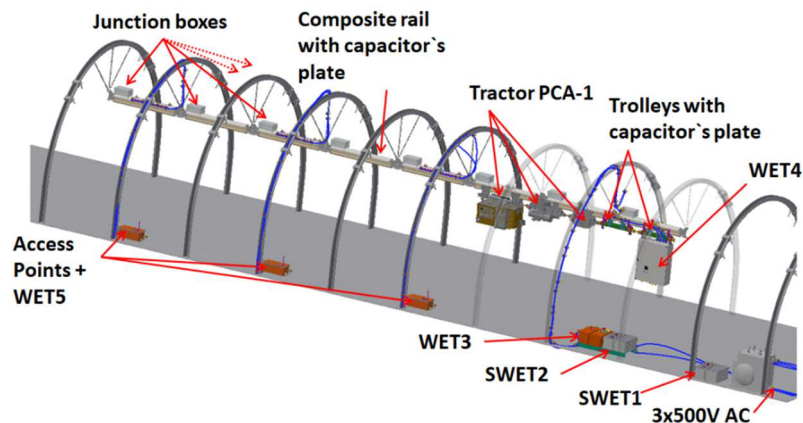

Fig. 19.Visualisation of the main modules associated with the WET system

In-situ tests of the prototype solution will be the next step of the HEET II project. For this purpose, a separate roadway is under preparation at the "Barbara" Experimental Mine, shown in Fig. 20.

Fig. 20. Space prepared for in-situ testing

In-situ tests of the system designed within the HEET II project, gave answers to many questions. Among the issues related to the WET system: the functional tests to determine the power transfer efficiency, measurement of stray currents and electric field strength in the vicinity of the composite rails containing the energy transfer capacitor plates should be realized. So far the analyses show that achieving the assumed power of the WET system depends on the capacitance of the capacitors (C_1, C_2 in Fig. 1). This capacitance depends on the distance between the plates, hence the tests of the impact of this distance on the parameters of the WET system are also planned. In order to achieve high power transfer rates, these distances should be as short as possible. On the other hand, due to the movement of the drivetrain on the suspended rails, including climbing hills, the air gap should be large enough to ensure that the receiving part is collision-free with the rails. An additional problem to be solved will be keeping the space between the plates clean under real conditions. The proposed system differs from standard solutions currently used in the mining industry, however, it should ensure safe operation, also in emergency states. Safety will be ensured from the selection of composite rail material meeting explosion-proof requirements (ATEX directive), through the protection of electronic parts in appropriate enclosures to dedicated control software responding to unusual operating states. All these issues will be subject to further work and tests.

References

Hanazawa, M., Sakai, N., & Ohira, T. (2012). SUPRA: Supply underground power to running automobiles: Electric Vehicle on Electrified Roadway exploiting RF displacement current through a pair of spinning tires. *2012 IEEE International Electric Vehicle Conference*. https://doi.org/10.1109/ievc.2012.6183164

Jeong, S. Y., Park, J. H., Hong, G. P., & Rim, C. T. (2019). Autotuning Control System by Variation of Self-Inductance for Dynamic Wireless EV Charging With Small Air Gap. *IEEE Transactions on Power Electronics*, 34(6), 5165–5174. https://doi.org/10.1109/TPEL.2018.2866412

Kianfar, A. E., Sherikar, M., Gilerson, A., Skora, M., Stankiewicz, K., Mitra, R., & Clausen, E. (2022). Designing a Monitoring System to Observe the Innovative Single-Wire and Wireless Energy Transmitting Systems in Explosive Areas of Underground Mines. *Energies*, 15(2), 576. https://doi.org/10.3390/en15020576

Konsek, R. (2012). Nowoczesny napęd akumulatorowy ciągnika PCA-1 jako alternatywa dla obecnie stosowanych napędów w ciągnikach transportowych (Modern battery-driven PCA-1 tractor as an alternative to the drives currently used in transport tractors). *Zeszyty Problemowe – Maszyny Elektryczne*, 2, 1–5 (in Polish).

Konsek, R., Kaczmarczyk, K., Budzyński, Z., & Polnik, B. (2013). Podwieszony ciągnik akumulatorowy PCA-1 (Battery suspended drivetrain PCA-1). *Napędy i Sterowanie*, 7/8, 112–115 (in Polish).

Kurpiel, W. (2020). Research on balancing BMS systems in a climatic chamber. *Mining Machines*, 3/2020(163), 53–63. https://doi.org/10.32056/KOMAG2020.3.6

Kracek, J., & Svanda, M. (2019). Analysis of Capacitive Wireless Power Transfer. *IEEE Access*, 7, 26678–26683. https://doi.org/10.1109/access.2018.2883712

Maji, S., Sinha, S., & Afridi, K. K. (2021). Roadway Embeddable Multi-MHz Capacitive Wireless Charging System with Matching Network Realized using Wiring Parasitics. *2021 IEEE Energy Conversion Congress and Exposition (ECCE)*, 5775–5780. https://doi.org/10.1109/ecce47101.2021.9595823

Mi, C. C., Buja, G., Choi, S. Y., & Rim, C. T. (2016). Modern Advances in Wireless Power Transfer Systems for Roadway Powered Electric Vehicles. *IEEE Transactions on Industrial Electronics*, 63(10), 6533–6545. https://doi.org/10.1109/tie.2016.2574993

Mohammed, S. A. Q., & Jung, J.-W. (2021). A Comprehensive State-of-the-Art Review of Wired/Wireless Charging Technologies for Battery Electric Vehicles: Classification/Common Topologies/Future Research Issues. *IEEE Access*, 9, 19572–19585. https://doi.org/10.1109/access.2021.3055027

Regensburger, B., Sinha, S., Kumar, A., Vance, J., Popovic, Z., & Afridi, K. K. (2018). Kilowatt-scale large air-gap multi-modular capacitive wireless power transfer system for electric vehicle charging. *2018 IEEE Applied Power Electronics Conference and Exposition (APEC),* 666–671. https://doi.org/10.1109/apec.2018.8341083

Stankiewicz, K. (2020). Mechatronic systems developed at the KOMAG. *Mining Machines*, 2, 59–68. https://doi.org/10.32056/KOMAG2020.2.6.

Sinha, S., Kumar, A., & Afridi, K. K. (2018). Improved design optimization of efficient matching networks for capacitive wireless power transfer systems. *2018 IEEE Applied Power Electronics Conference and Exposition (APEC)*, 3167–3173. https://doi.org/10.1109/apec.2018.8341554

Vu, V.-B., Dahidah, M., Pickert, V., & Phan, V.-T. (2020). An Improved LCL-L Compensation Topology for Capacitive Power Transfer in Electric Vehicle Charging. *IEEE Access*, 8, 27757–27768. https://doi.org/10.1109/access.2020.2971961

Zhang, H., Lu, F., & Mi, C. (2020). An Electric Roadway System Leveraging Dynamic Capacitive Wireless Charging: Furthering the Continuous Charging of Electric Vehicles. *IEEE Electrification Magazine*, 8(2), 52–60. https://doi.org/10.1109/mele.2020.2985486

Zhang, H., Zhu, C., & Lu, F. (2019). Long-Distance and High-Power Capacitive Power Transfer based on the Double-Sided LC Compensation: Analysis and Design. *2019 IEEE Transportation Electrification Conference and Expo (ITEC)*, 1–5. https://doi.org/10.1109/itec.2019.8790595

Zhang, Z., Pang, H., Georgiadis, A., & Cecati, C. (2019). Wireless Power Transfer—An Overview. *IEEE Transactions on Industrial Electronics*, 66(2), 1044–1058. https://doi.org/10.1109/TIE.2018.2835378

Zygmanowski, M., Kasprzak, M., Kierepka, K., Michalak, J., Jarek, G., & Przybyla, K. (2021). Power Loss Analysis of Multi-converter System with Single Wire and Wireless Energy Trasfer. *2021 International Conference on Electrical Drives & Power Electronics (EDPE)*, 1–6. https://doi.org/10.1109/edpe53134.2021.9604052